Structural evolution of calcium sodium aluminosilicate hydrate (C-(N-)A-S-H) gels induced by water exposure

The impact of Na leaching

Liu, Chen; Li, Zhenming; Nie, Shuai; Skibsted, Jørgen; Ye, Guang

DOI
10.1016/j.cemconres.2024.107432

Publication date
2024

Document Version
Final published version

Published in
Cement and Concrete Research

Cement and Concrete Research 178 (2024) 107432

Contents lists available at ScienceDirect

Cement and Concrete Research

journal homepage: www.elsevier.com/locate/cemconres

Structural evolution of calcium sodium aluminosilicate hydrate (C-(N-)A-S-H) gels induced by water exposure: The impact of Na leaching

Chen Liu [a], Zhenming Li [b,c,d], Shuai Nie [e,*], Jørgen Skibsted [e], Guang Ye [a,*]

[a] Department of Materials and Environment (Microlab), Faculty of Civil Engineering and Geoscience, Delft University of Technology, 2628 CN Delft, Netherlands
[b] School of Civil and Environmental Engineering, Harbin Institute of Technology, 518055 Shenzhen, China
[c] Guangdong Provincial Key Laboratory of Intelligent and Resilient Structures for Civil Engineering, Harbin Institute of Technology, 518055 Shenzhen, China
[d] Department of Materials Science and Engineering, The University of Sheffield, S13JD Sheffield, United Kingdom
[e] Department of Chemistry and Interdisciplinary Nanoscience Center (iNANO), Aarhus University, 8000 Aarhus C, Denmark

ARTICLE INFO

Keywords:
C-(N-)A-S-H gel
Water immersion
Leaching
Structural evolution
^{23}Na, ^{27}Al and ^{29}Si NMR

ABSTRACT

Calcium sodium aluminosilicate hydrate C-(N-)A-S-H gels, formed through the alkali-activation of calcium silicate-based materials, may exhibit greater susceptibility to aqueous environments when compared to traditional C-(A-)S-H phases formed by hydration of blended Portland cements. This study investigates structural changes in synthesized C-(N-)A-S-H gels triggered by water immersion. Three gels have been examined, each with stoichiometrically controlled ratios of Ca/Si (0.8 and 1.2), Al/Si (0.1 and 0.3), and Na/Si (0.1, 0.2, and 0.3). The gel with a higher Ca/Si ratio demonstrated enhanced resistance to water leaching and only experienced marginal decalcification whereas the gels with lower Ca/Si ratios exhibited more pronounced effects including leaching losses of Si. Notably, all gels displayed rapid and substantial sodium leaching, contributing to an increased degree of polymerization for the aluminosilicate tetrahedra in the gels. A plausible mechanism for this change is that Na leaches out from the interlayer and Ca ions progressively take over the role of charge compensators in the interlayer of the C-(N-)A-S-H structure.

1. Introduction

Society's concern regarding global warming continues to increase and promote research in alternative materials with lower CO_2 footprint, in particular materials for the construction industry. In this context, alkali-activated slag (AAS) materials have attracted substantial attention in both academic and engineering fields [1–3], since AAS binders hold considerable potential for reductions of energy consumption and carbon emissions compared to conventional Portland cement (PC). Additionally, AAS materials usually exhibit desirable mechanical properties, as a result of a dense microstructure, and even superior durability at certain specific conditions, as compared to other cementitious materials [4–6]. Consequently, AAS binder is emerging as a promising supplement to traditional cement in the building construction sector, although the availability of slag is decreasing.

Nonetheless, several challenges persist with applications of AAS materials, including leaching which commonly occurs when these materials are exposed to humid or aqueous conditions. Contrary to ordinary Portland cement binders, which may undergo further hydration in a moist environment, the introduction of external water not only fails to promote further reaction of the precursors but also leads to alkali depletion in the pore solution, thereby compromising the properties of AAS materials. For example, a reduced compressive strength and coarsened pore structure have been reported for alkali-activated fly ash-slag pastes upon exposure to water, as compared to pastes under sealed conditions [7]. Similar results were also found by Huang et al. [8] for alkali-activated mortars produced from municipal solid waste incinerator bottom ash, which exhibited diminished compressive strength under standard fog and soaking conditions as compared to sealed conditions. In our recent work [9], degradations of AAS pastes subjected to long-term water immersion, including microstructure deterioration and gel decomposition, were also observed. Thus, it appears that the C-(N-)A-S-H gels in AAS system are more vulnerable to underwater conditions than those of C-(A-)S-H phases in conventional cementitious systems, and therefore these gels should be investigated in more detail to gain a deeper understanding of the underlying degradation mechanisms.

In comparison to the C-(A-)S-H phases formed in PC systems, C-(N-)A-S-H gels present in AAS systems generally possess lower Ca/(Si + Al)

* Corresponding authors.
E-mail addresses: shuainie@chem.au.dk (S. Nie), G.Ye@tudelft.nl (G. Ye).

https://doi.org/10.1016/j.cemconres.2024.107432
Received 20 November 2023; Received in revised form 28 December 2023; Accepted 11 January 2024
Available online 28 January 2024

Table 1
Optimized proportions of reaction solutions for the C-(N-)A-S-H gel synthesis (in mL).

	0.6 M Na_2SiO_3	0.24 M $Ca(NO_3)_2$	0.12 M $Al(NO_3)_3$	10 M NaOH	Deionized H_2O	Targeted Ca/Si	Targeted Al/Si
0.8_0.1	80	100	40	50	80	0.8	0.1
0.8_0.3	80	100	120	50	–	0.8	0.3
1.2_0.3	50	150	75	50	25	1.2	0.3

Table 2
Chemical composition (wt%) and elemental molar ratios for the synthesized C-(N-)A-S-H gels.

	CaO	SiO_2	Al_2O_3	Na_2O	Ca/Si	Al/Si	Na/Si	Na/Al
0.8_0.1	41.7	49.4	4.1	4.7	0.90	0.10	0.18	1.87
0.8_0.3	37.2	45.9	9.4	7.5	0.87	0.24	0.32	1.31
1.2_0.3	48.9	42.3	7.4	1.4	1.24	0.21	0.07	0.32

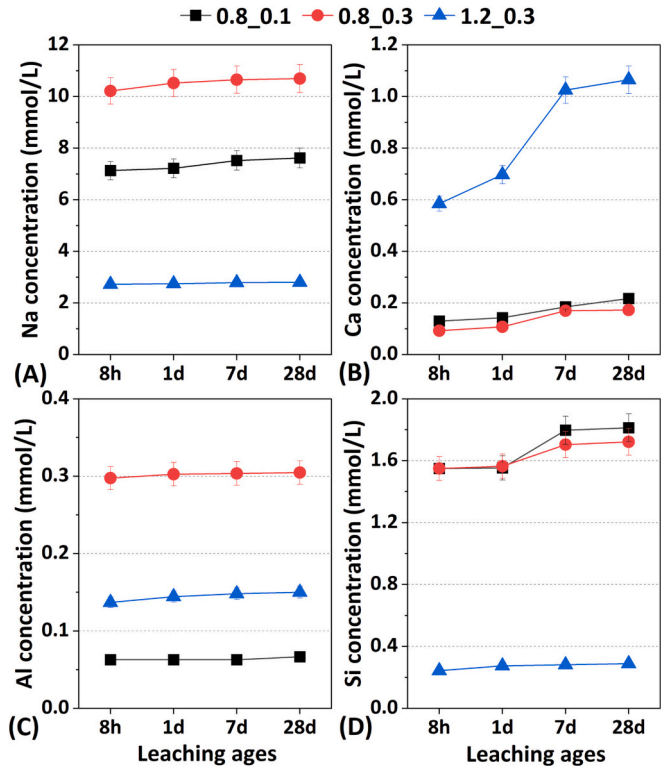

Fig. 1. Ion concentrations of Na, Ca, Al and Si in the leachates of the three C-(N-)A-S-H gels exposed to water and synthesized with Ca/Si = 0.8 and Al/Si = 0.1 (black squares), Ca/Si = 0.8 and Al/Si = 0.3 (red circles), and Ca/Si = 1.2 and Al/Si = 0.3 (blue triangles). The error bars, showing the standard deviations, are for some of the measurements below the size of the symbols for the measured values. (For interpretation of the references to color in this figure legend, the reader is referred to the web version of this article.)

ratios (0.6–1.2), higher Al/Si ratios (0.1–0.3) and high alkali uptakes [3,10–15]. These variations in chemical composition may lead to differences in gel structure and associated physico-chemical properties. Myers et al. [12] proposed a cross-linked substituted tobermorite-based model as a generalized structure for C-(N-)A-S-H gels. The interplay between composition, solubility, and structure of C-(N,K-)A-S-H gels has been investigated [13] and showed that the interlayer space of the tobermorite-like structure accommodates both Na^+ and K^+ ions and that a higher alkali content results in a lower Ca content in the interlayers. Furthermore, a high substitution degree of Si by Al can considerably enhance the mean chain length and polymerization degree of the alumino-silicate tetrahedra in C-(N-)A-S-H gels. Garg et al. [16]

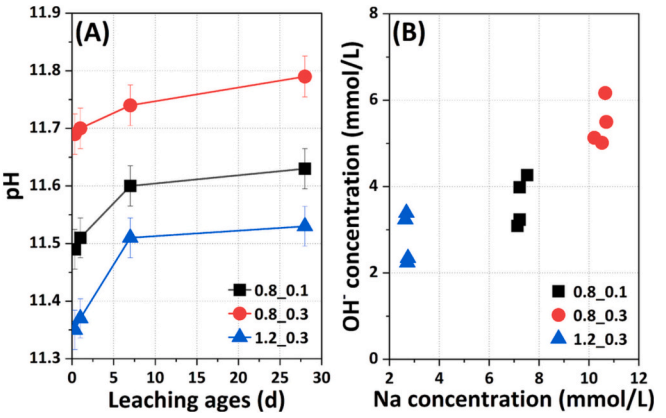

Fig. 2. (A) pH evolution of the leachates for the three C-(N-)A-S-H gels with exposure time. (B) Correlation between the concentrations of Na^+ and OH^- ions in the leachates for the C-(N-)A-S-H gels at the three different exposure times.

investigated the effect of Na^+ and K^+ ions on the nanoscale structure of C-S-H gels and found that the incorporation of alkalis resulted in consistent reductions in mean silicate chain length, polymerization degree of silicate tetrahedra, and basal spacing in the XRD patterns. Moreover, Yan et al. [17] reported that external immersion of C-S-H samples in NaOH/KOH solutions can increase the interlayer distance of the C-S-H gels.

Earlier studies have investigated the influence of leaching under acid attack conditions on the properties of C-(A-)S-H gels. Liu et al. [18] studied the impact of decalcification on structural and mechanical characteristics of synthesized C-S-H gels immersed in NH_4NO_3 solutions. Their results revealed that decalcification only occurs within the interlayer space, resulting in a reduction in stiffness along the c-axis. Notably, despite significant alterations in the linkage of silicate chains, the incompressibility and transverse isotropy of the calcium-silicate layers remained stable. Wang et al. [15] have studied the degradation mechanisms of C-(N-)A-S-H and N-A-S-H gels exposed to acidic conditions and found that both types of gels exhibit a detectable dealumination where almost all Al(IV) transferred into Al(VI) during exposure to sulfuric acid. Furthermore, both gels demonstrated increased silicate polymerization after acid immersion, in particular for the C-(N-)A-S-H gels.

As mentioned above, AAS materials also show clear degradations under water immersion [9,19]. However, investigations of structural changes for C-(N-)A-S-H gels subjected to water immersion have not been reported so far. This may reflect that C-(A-)S-H gels in conventional cementitious systems are considered structurally robust towards water immersion, and therefore leaching of C-(A-)S-H gels under water conditions has not attracted significant concerns. The influence of Na on the structure of C-(N-)A-S-H gels has frequently been overlooked, and this oversight can be attributed, in part, to earlier research findings indicating a relatively weak bonding of Na within the gel matrix [20], leading to the assumption that Na plays a negligible role in the development of the gel structure. Consequently, the impact of Na leaching and associated structural changes of the C-(N-)A-S-H gels may have been overlooked.

The objective of this study is to provide an analysis of the structural changes occurring in C-(N-)A-S-H gels when subjected to water immersion. To achieve this, we use three synthesized C-(N-)A-S-H gels with

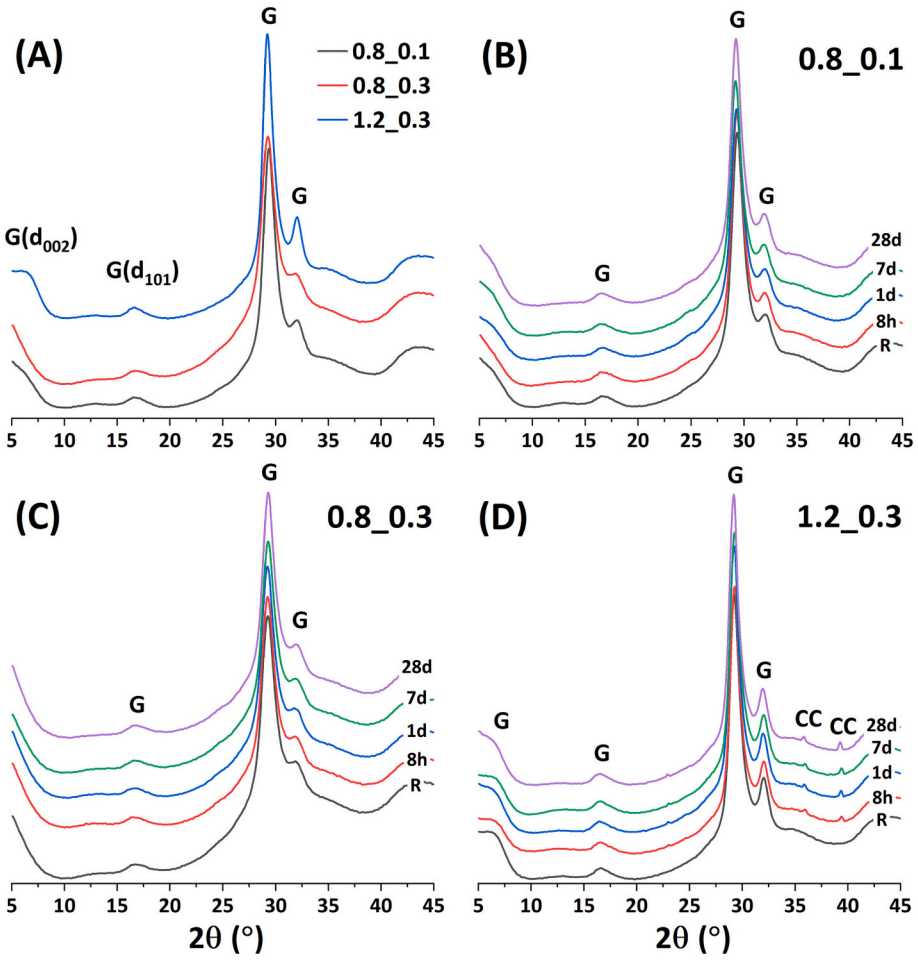

Fig. 3. (A) Powder XRD diffractograms of the three unexposed C-(N-)A-S-H gels. (B–D) XRD patterns for the three C-(N-)A-S-H gels at different leaching times. G: C-(N-)A-S-H gel; CC: calcium carbonate.

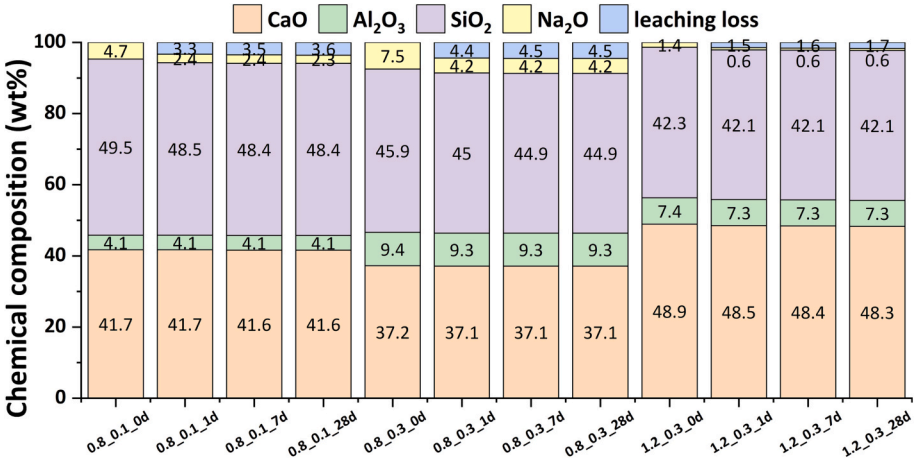

Fig. 4. Chemical compositions of the C-(N-)A-S-H gels before and after water immersion for 1, 7, and 28 days. The leaching loss is calculated using the ICP results of the leachates for gels.

distinct Ca/Si and Al/Si ratios, i.e., 0.8 and 0.1, 0.8 and 0.3, and 1.2 and 0.3, respectively, which collectively span the representative ranges for these elements in AAS systems [3]. The synthesis process was carried out under high-pH conditions similar to those found in real AAS systems [21–23]. Subsequently, the synthesized gels were immersed in deionized water for varying exposure durations, and the leaching processes were tracked by measuring ion concentrations in the leachates. Furthermore, solid materials were isolated, and relationships between leaching behaviour and structural change of the gels were established. Overall, this study aims to deepen our comprehension of the degradation mechanism of AAS materials in aqueous environments, with a primary emphasis on the structure and composition of the C-(N-)A-S-H gel.

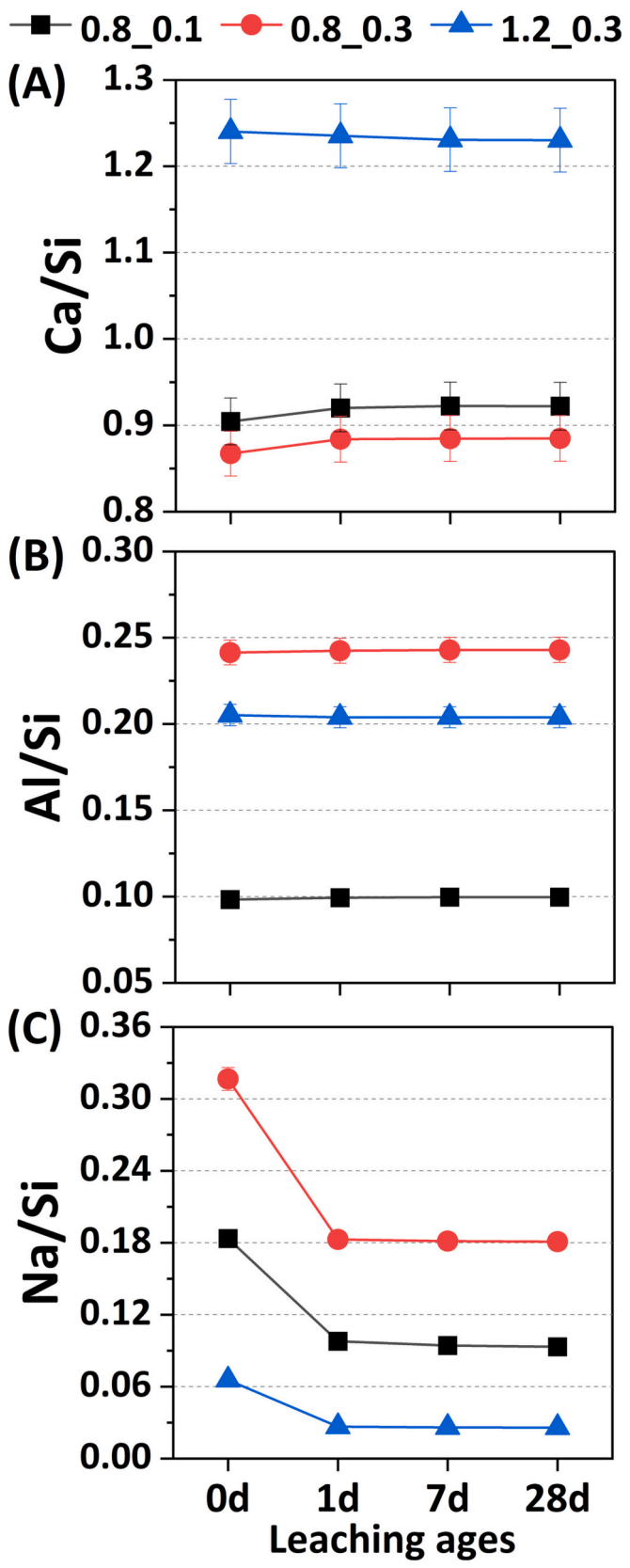

Fig. 5. Molar Ca/Si, Al/Si and Na/Si ratios for the C-(N-)A-S-H gels at different leaching ages. The error bars, showing the standard deviations, are for some of the measurements below the size of the symbols for the measured values.

2. Materials and methods

2.1. Materials

The synthesis of C-(N-)A-S-H gels was conducted using the widely employed double decomposition method, as described in detail in previous studies [24–28]. This approach produces gels that exhibit comparable characteristics to those resulting from direct reactions of the various oxides in solution [29]. Moreover, it provides enhanced synthesis efficiency and the capability to mitigate potential interference from unreacted raw materials. For this study, three distinct stoichiometrically tailored gels were synthesized, denoted as 0.8_0.1, 0.8_0.3, and 1.2_0.3, where the values of 0.8 and 1.2 correspond to the targeted Ca/Si ratios, whereas 0.1 and 0.3 are the targeted Al/Si ratios. The comparison between the former two gels aimed to elucidate the impact of the Al/Si ratio on gel leaching, while that involving the latter two was designated to investigate the influence of Ca/Si ratios on gel leaching.

The gel syntheses were carried out using solutions of 0.6 M $Na_2SiO_3{\cdot}5H_2O$, 0.24 M $Ca(NO_3)_2{\cdot}4H_2O$, 0.12 M $Al(NO_3)_3{\cdot}9H_2O$, and 10 M NaOH, the latter utilized for pH adjustment. All solutions were prepared using deionized water as the solvent. The proportions of the solutions were tailored to the targeted elemental ratios presented in Table 1. It should be noted that the high solubility of Si and Al and low solubility of Ca under high alkaline conditions [30] imply that the molar Ca/Si ratios calculated from the reactants are lower than the targeted Ca/Si ratios in gels. The optimization of the proportions of the solutions for the gel synthesis (Table 1) was carried out through a systematic approach which involved a step-by-step comparison between the targeted Ca/Si and Al/Si ratios and the actual values determined from XRF analysis.

High-purity N_2 from a gas cylinder was progressively released into the glove box containing all experimental setups for at least 20 mins, with the valve opened to the external environment. This process aimed to exhaust any residual air present in the glove box. Then, the valve was closed and the recirculation mode was initiated, which allowed the whole gel synthesis process to be carried out under a pure N_2 atmosphere with standard atmospheric pressure. The solutions were carefully added drop-by-drop into a conical flask following the order of NaOH, Na_2SiO_3, $Al(NO_3)_3$, $Ca(NO_3)_2$, and deionized water [26], and constant stirring was applied for 7 days in the sealed conical flasks to maintain a constant environment [31]. Following the experiments, the valve was reopened and all the sample and reactor were removed. Both the supernatant and the newly formed gels were collected following centrifugation. The pH values of the supernatant from the 0.8_0.1, 0.8_0.3, and 1.2_0.3 gels were 14.2, 14.1, and 14.1, respectively, as measured by titration. These pH values align with the pH of pore solutions in real AAM systems [9,32]. To further purify the freshly formed gels, a thorough washing procedure was applied. This involved three successive treatments with deionized water (500 mL each time) and a single wash with absolute alcohol (500 mL). Each washing cycle took place in an ultrasonic bath for 2 min. Subsequent to the washing, the gel samples were freeze-dried for 3 days. Afterwards, the gels were finely ground into powders and stored in a desiccator prior to the measurements [11,17,33], where the desiccator contained a saturated $CaCl_2$ solution (relative humidity (RH) ≈ 30 %) and solid NaOH serving as a CO_2 trap.

The chemical compositions and the corresponding Ca/Si and Al/Si ratios of the three synthesized C-(N-)A-S-H gels (Table 2) were determined by X-ray fluorescence (XRF). The obtained Ca/Si ratios are slightly higher than the target values, whereas the Al/Si ratios are lower. In addition, the presence of Na is also identified in all three C-(N-)A-S-H gels.

For the leaching experiments under water-exposed conditions, 1.500 g (± 0.001 g) of gel was mixed with 150.0 g (± 0.1 g) of deionized water in a sealed polyethene bottle. The samples were allowed to equilibrate at room temperature (25 ± 2 °C) and shaken twice a week [13]. After immersion for designated ages of 8 h, 1 d, 7 d and 28 d, the gels were

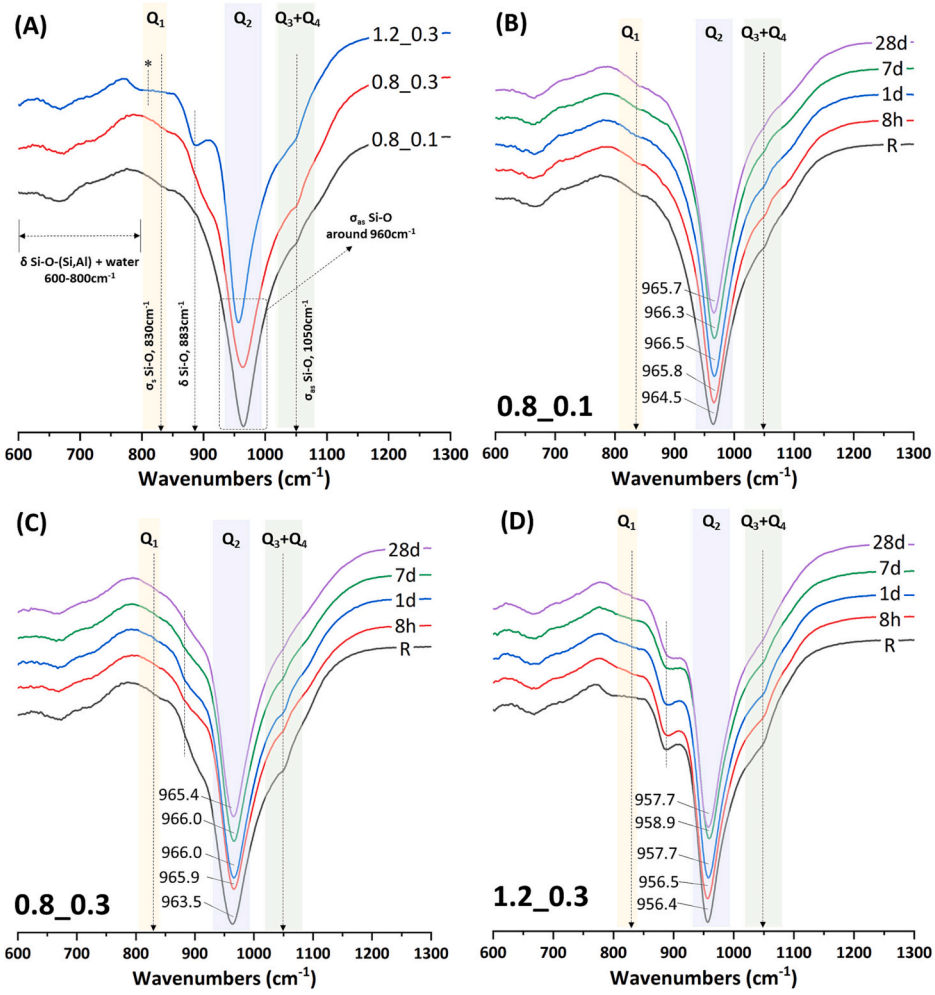

Fig. 6. (A) FTIR spectra of the C-(N-)A-S-H gels before leaching. (B–D) FTIR spectra of the three C-(N-)A-S-H gels following the time evolution of leaching. δ indicates bending vibrations, σ_{as} asymmetric stretching vibrations, and σ_s symmetric stretching vibrations. R indicates the reference samples before leaching whereas the other spectra are denoted by their leaching times (8 h, 1 d, 7 d, and 28 d).

filtrated and washed with absolute alcohol for five times. Subsequently, the leached gels were subjected to the same drying and storage procedures as described above for the synthesized samples. The leachates of the gels were centrifuged, and the resulting supernatants were collected for further ion concentration analysis.

2.2. Methods

2.2.1. Aqueous phase characterizations

The ion concentrations of Na, Ca, Si, and Al in the leachates were quantified using a PerkinElmer Optima 5300DV inductively coupled plasma optical emission spectrometry (ICP-OES) instrument. The pH values of the host solutions (>14), mentioned above, were determined through titration against 0.1 mol/L of HCl acid, employing phenolphthalein as an indicator, whereas the pH values of the leachates were measured by a pH meter from Metrohm, Switzerland.

2.2.2. Solid phase characterizations

Characterization of the powdered C-(N-)A-S-H gels, both before and after leaching, was carried out by several analytical techniques, including XRF, X-ray diffraction (XRD), Fourier-transform infrared spectroscopy (FTIR) and solid-state magic-angle spinning (MAS) nuclear magnetic resonance (NMR) spectroscopy. For quantitative determination of the elemental composition of the C-(N-)A-S-H gel after leaching, the XRF measurements were conducted using a Panalytical Axios Max WD-XRF spectrometer. For the powder XRD measurements, a Bruker D8 Advance diffractometer with CuKα radiation (1.54 Å) was employed, with a step size of 0.02° and a dwell time of 5 s per step. The FTIR measurements were performed on a Nicolet™ iS50 FTIR Spectrometer, where the wavenumber range spanned from 600 to 4000 cm^{-1} with a resolution of 4 cm^{-1}. A total of 20 scans were collected per sample.

The single-pulse ^{29}Si MAS NMR spectra were acquired at 79.4 MHz on a Bruker Avance 400 NMR (9.4 T) spectrometer, using a 4 mm Bruker CP/MAS probe with a spinning frequency of $\nu_R = 10.0$ kHz, a 45° excitation pulse ($\gamma B_1/2\pi = 71$ kHz), a relaxation delay of 30 s, and 5600 scans. ^{29}Si chemical shifts are referenced to tetramethylsilane (TMS), using β-Ca_2SiO_4 ($\delta(^{29}Si) = -71.33$ ppm [34]) as a secondary reference. The deconvolutions of the ^{29}Si MAS NMR spectra were carried out by least-squares fitting using a combination of Gaussian and Lorentzian peak shapes and MATLAB® codes implemented in a recent study [35]. The ^{23}Na and ^{27}Al MAS NMR spectra were recorded on a narrow-bore Bruker Avance 950/54 us^2 NMR spectrometer (22.3 T), employing a triple-resonance ^1H-X-Y 2.5 mm Bruker CP/MAS probe with a spinning frequency of $\nu_R = 25.0$ kHz, a pulse width of 0.5 μs for rf field strengths of $\gamma B_1/2\pi = 81$ kHz and 100 kHz for ^{23}Na and ^{27}Al, respectively, a relaxation delay of 2 s, ^1H decoupling ($\gamma B_2/2\pi = 70$ kHz) during acquisition, and typically 4096 scans. ^{23}Na and ^{27}Al isotropic chemical shifts were referenced to external samples of 1.0 M aqueous NaCl and $AlCl_3 \bullet 6H_2O$ solutions, respectively.

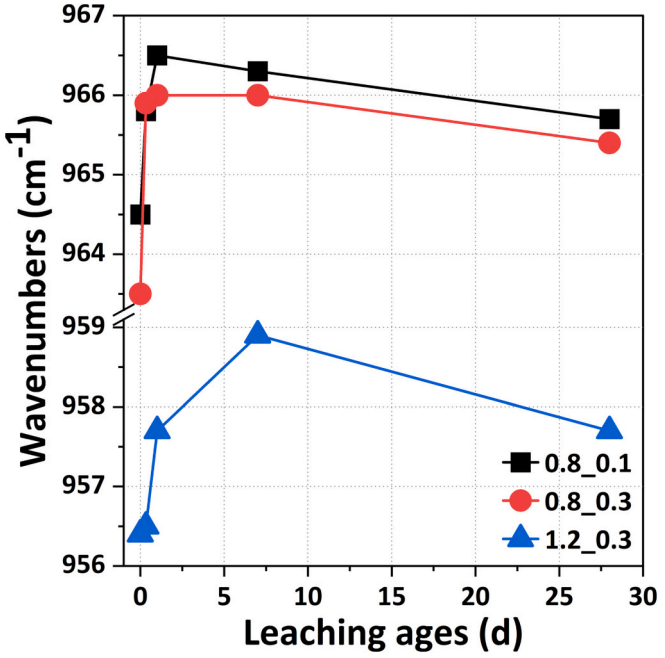

Fig. 7. Changes of the FTIR wavenumbers for the asymmetric stretching vibration of Si—O bonds in Q^2 sites of the C-(N-)A-S-H gels as a function of the leaching time.

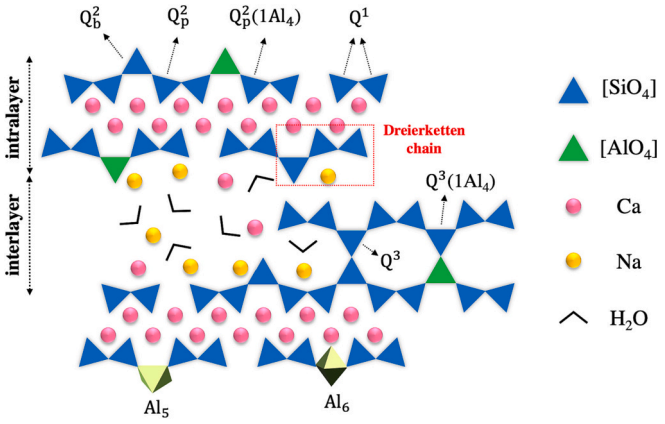

Fig. 8. Schematic model for the structure of a C-(N-)A-S-H gel based on the defect tobermorite model and emphasizing the local environment of various silicate and aluminate species. It should be noted that five- (Al_5) and six-fold (Al_6) coordinated Al are only present in gels with high Ca/Si ratios (i.e., Ca/Si $\geq$ 1.2 [47]).

3. Results and discussion

3.1. Ions concentrations in leachate

The evolution of ion concentrations for Na, Ca, Al and Si in the leachate of the C-(N-)A-S-H gels exposed to water is shown in Fig. 1 as a function of the leaching time. The predominant ions in the leachate are Na, followed by Si, Ca, and Al. The concentration of Na appears to stabilize after 1 day (Fig. 1A), indicating that a significant portion of Na can rapidly leach away from the gels. Since the fresh gels have been centrifuged and ultrasonically washed four times, this loss of Na is primarily attributed to the release of charge-balancing Na from the interlayer rather than physically absorbed Na on the surface of gels. This observation aligns with earlier studies [14,36], suggesting that Na is weakly bonded in the basal spacing of C-(N-)A-S-H gels. Furthermore, it is apparent that the Na concentration in the leachate exhibits a positive correlation with the initial Na content in the unexposed C-(N-)A-S-H gels (*c.f.* Table 2), which decreases with increasing Ca/Si ratio for a fixed Al/Si ratio [37].

In contrast to Na, the Ca ions leach with a slower rate (Fig. 1B), indicating a stronger binding of the interlayer Ca ions to the aluminosilicate chains. The concentration of Ca reveals a gradual increase over time for all three samples with the highest leaching observed for the 1.2_0.3 gel with the highest initial Ca content. Additionally, dissolution of Al is detected, with the quantity of dissolved Al also being proportional to the initial Al content in the solid phase (Fig. 1C). Al shows a similar leaching behaviour as Na, with no changes in concentration after 8 h of water exposure. The leaching behaviour for Si resembles that of Ca, with the equilibrium concentration of Si at 28 days being higher than Ca in the gels with a low Ca/Si ratio (e.g., Ca/Si $<$ 1; Fig. 1D). The dissolved Ca to Si molar ratios in the leachates are 3.7 for the 1.2_0.3 gel after 28 days of water immersion and 0.1 for the gels with Ca/Si = 0.8. This suggests an incongruent leaching of Ca and Si, where the gel with the higher Ca content has a larger loss of Ca along with a comparatively lower loss of Si. The initial Na content in the 1.2_0.3 gel is lower than that in the 0.8_0.3 gel, indicating that a larger portion of Ca acts as a charge compensator to balance the negative charges resulting from the substitution of Si by Al in the silicate chains and the more disrupted alumino-silicate chains present at higher Ca/Si ratio [37]. Since the interlayer Ca is more susceptible to leaching than Ca in the principal layers, a higher loss of Ca is observed for the 1.2_0.3 gel. Overall, C-(N-)A-S-H gels under water-exposed conditions reveal distinct leaching behaviours for the different ions, which may partly reflect the Ca/Si, Al/Si and Na/Si ratios of the gels as illustrated in Fig. A1.

The pH evolution of the leachates is depicted in Fig. 2A as a function of exposure time and shows that the pH of the leachate increases with the dissolution of the C-(N-)A-S-H gels, reaching values over 11.5 after 28 days of water immersion. The formation of C-(N-)A-S-H gels involves a series of alkali-consuming reactions and aqueous ions of Ca^{2+}, Na^+, $[Al(OH)_4]^-$, $[SiO(OH)_3]^-$ and $[SiO_2(OH)_2]^{2-}$. Reversely, the disintegration of C-(N-)A-S-H gels in water is supposed to be an alkali-releasing process. Since the concentration of Na is much higher than that of Ca, Si, and Al in the leachate, the pH of the leachate is mainly controlled by the initial content of Na in the solids. Therefore, the gels containing more alkali ions (the 0.8_0.1 and 0.8_0.3 gels) have higher leakages of OH^- ions. Indeed, Fig. 2B confirms that the concentration of OH^- in the leachates correlates positively with the aqueous Na concentration.

3.2. Solid phase composition

The XRD patterns for the three C-(N-)A-S-H gels, prior to water exposure, are shown in Fig. 3A and include four distinct peaks, characteristic for the C-(N-)A-S-H gels, are comparable with the reflections observed for poorly-ordered analogues of orthorhombic 14-Å tobermorite (PDF# 00-029-0331) [17]. These peaks are roughly positioned at 2θ values of 5 – 7°, 17°, 29°, and 32°, which resemble the XRD reflections of representative C-(N-)A-S-H gels in real AAS pastes [9,22,23]. The lowest reflection (d_{002}) is related to the basal spacing of the gel [38]. However, the basal spacings of calcium aluminosilicate hydrate gels are highly dependent on the chemical composition of the gels [33,39,40], where an increase in Al content or a decrease in Ca content can lead to a broader basal spacing. Moreover, a higher water content in the gels can also contribute to the expansion of basal spacing [33]. Only limited information about the basal spacings can be extracted from the patterns in Fig. 3A, since no distinguishable peaks can be identified in the range from 5 to 10° (i.e., only a broad hump is observed for the Ca/Si = 1.2 gel). This can mainly be attributed to the preference for the formation of amorphous phases for gels with high Al and low Ca contents [16,17].

The poorly crystalline C-(N-)A-S-H gels (0.8_0.1 and 0.8_0.3) also exhibit lower intensity of the characteristic peaks around 29° and 32° when compared to the 1.2_0.3 gel. The d_{101} reflections observed for all

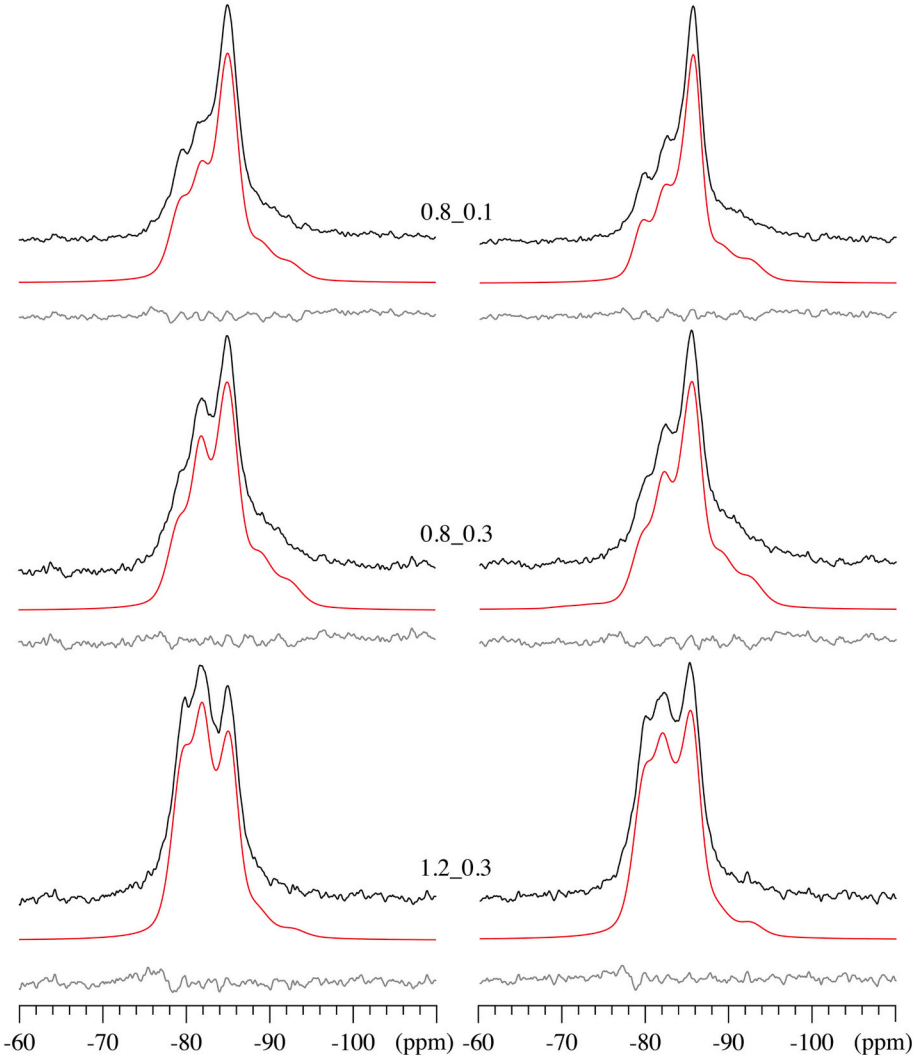

Fig. 9. ^{29}Si MAS NMR spectra (9.4 T, ν_R = 10.0 kHz) of the three C-(N-)A-S-H gels before leaching (left) and after immersion in water for 28 days (right). The experimental spectra are shown in black, optimized simulated spectra in red, and difference spectra in grey. (For interpretation of the references to color in this figure legend, the reader is referred to the web version of this article.)

three gels are indicative of bridging Si sites, which may suggest C-(N-)A-S-H gels with cross-linked structures [41]. No significant structural changes are detected by XRD for the three C-(N-)A-S-H gels upon leaching duration, as shown in Fig. 3B–D. However, minor peaks from calcium carbonate are detected in the 1.2_0.3 gel, which is consistent with results from TGA and may be expected for gels with high Ca/Si ratios. These findings suggest that water leaching only leads to changes that has a minimal influence on the overall structure of the gels.

Changes in chemical composition of the C-(N-)A-S-H gels over the leaching period are shown in Fig. 4, as determined from XRF measurements. It is observed that the two gels with low Ca/Si ratio have higher weight losses than the 1.2_0.3 sample, which is primarily a result of a higher leaching of Na and Si. The rapid and significant leaching of Na ions is a result of the higher mobility of Na as compared to the other ions, where the highest loss is observed for the 0.8_0.3 sample with the highest initial Na content. The highest loss in Si contents is observed for the gels with the lowest Ca/Si ratios (although small) and may potentially reflect the presence of longer alumino-silicate chains rather than a preference of dimers, as present in high Ca/Si ratio gels. Considering that the Ca/Si ratio of C-(A-)S-H phases in cement systems is higher than that of C-(N-)A-S-H gels in AAS systems [3], it is plausible that the leaching stability of C-(N-)A-S-H gels is less robust. Therefore, this result can well explain the phenomenon of gel decomposition in AAS pastes after long-term water immersion [9].

The Ca/Si, Al/Si, and Na/Si ratios for the C-(N-)A-S-H gels, before and after water exposure and calculated from the data in Fig. 4, are shown in Fig. 5. No variations in the Ca/Si and Al/Si ratios can be observed with exposure time, within the uncertainty limits of the data. For the Al/Si ratios, this indicates a congruent dissolution of Si and Al during water leaching. As for the Na/Si ratios, the three C-(N-)A-S-H gels all show a Na loss within the first day of leaching, after which the values stabilize and become invariant for the remaining exposure time. As shown in Fig. 5(C), the gel with a higher Al/Si ratio appears to show a higher Na/Si ratio before and after leaching, as compared with the gels of 0.8_0.1 and 0.8_0.3. This indicates that the gel with a higher Al incorporation is more effective in the immobilization of Na.

3.3. Solid phase structure

3.3.1. FTIR

FTIR spectra of the C-(N-)A-S-H gels before and after leaching are shown in Fig. 6A and include five distinct regions that can be related to Si—O bondings. The wavenumbers ranging from 600 to 800 cm^{-1} correspond to bending vibrations of Si-O-Si(Al) groups within calcium aluminosilicate hydrates and the vibration of water molecules [40]. The bands in the range from 800 to 1200 cm^{-1} are assigned to vibrations of

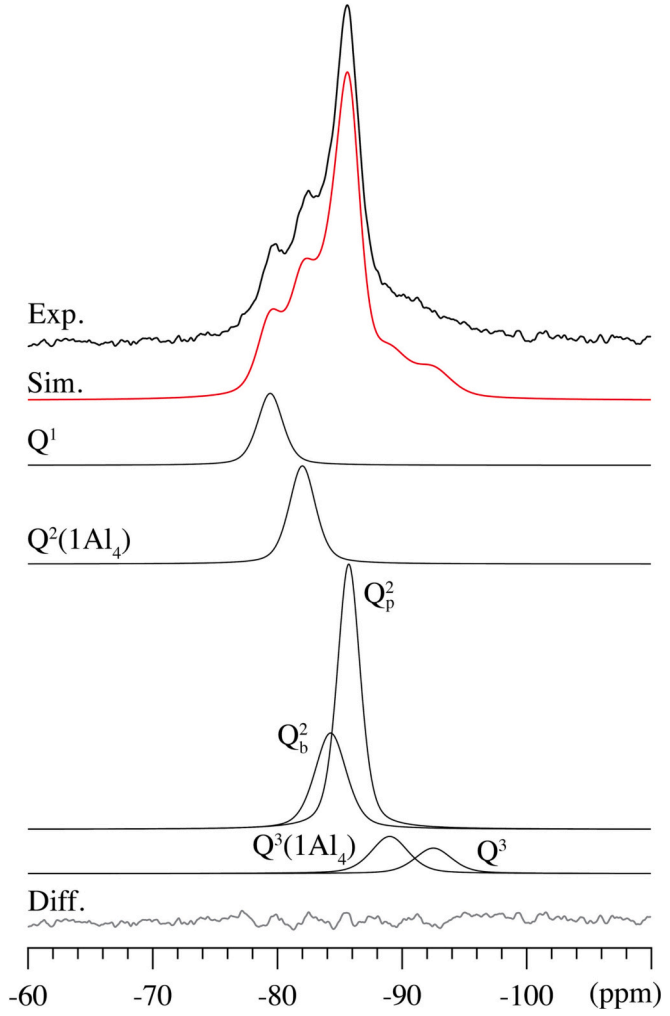

Fig. 10. ^{29}Si MAS NMR spectrum (9.4 T, $\nu_R = 10.0$ kHz) of the 0.8_0.1 C-(N-)A-S-H gel after leaching for 28 days along with its optimized simulation. The individual components of the simulated spectrum are shown below along with their assignment.

Si—O groups [42,43]. More specifically, the band at approximately 830 cm^{-1} is related to the symmetric stretching vibrations of the Si—O bonds [44] associated with the Q^1 sites within the dreierketten chains [45]. However, no significant differences in these stretching vibrations for the Q^1 sites are observed for the different gels from the FTIR spectra. A minor shoulder, indicated by the asterisk in Fig. 6A, positioned at a lower frequency relative to the Q^1 peak is seen for the 1.2_0.3 gel. This signal was also observed for C-S-H phases by Yan et al. [17], however, an assignment of the signal has not been proposed. The band at 883 cm^{-1} corresponds to the bending vibration of Si—O [46], and the 1.2_0.3 gel exhibits a more pronounced intensity at this wavenumber relative to the other two gels. This difference could potentially be ascribed to a more ordered structure of the 1.2_0.3 gel, as a result of the higher Ca content in the gel. The most clear and well-defined peak around 960 cm^{-1} represents the asymmetric stretching vibration of Si—O bonds within the "fingerprint region" for Q^2 sites [17]. It is noteworthy that the shift towards lower wavenumbers for the Q^2 peak indicates a decrease in the polymerization degree of the C-(N-)A-S-H gel [43], in agreement with that the 1.2_0.3 gel with a high Ca/Si ratio exhibits a less polymerized structure. The asymmetric Si—O stretching vibration located at 1050 cm^{-1} is ascribed to Si—O in Q^3 sites, and the intensity at this wavenumber is higher for both the 1.2_0.3 and 0.8_0.3 gels than for the 0.8_0.1 gel, which suggests that the gels with higher Al/Si ratio tend to have more crosslinked structures, in accordance with earlier findings for

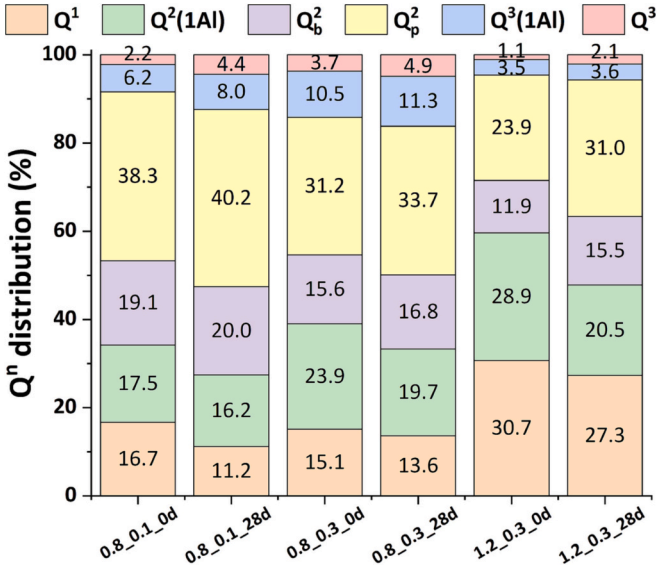

Fig. 11. Distribution of intensities for the distinct SiO_4 environments for the C-(N-)A-S-H gels before and after 28 days of leaching, as determined from simulations of the ^{29}Si NMR spectra in Fig. 9.

alkali-activated slag cements [41].

The time evolution of leaching is followed by the FTIR spectra in Fig. 6B–D for the three C-(N-)A-S-H gels. These spectra show no additional signals, as compared to those before leaching, indicating that no new phases are formed and that variations in intensity reflect minor structural rearrangements, predominately of Q^n species, in the C-(N-)A-S-H gels. The signals from the Q^1 sites are very similar for all leaching times, whereas progressive changes are evident for the Q^2 sites (peak around 960 cm^{-1}) as shown in Fig. 7. All three C-(N-)A-S-H gels display similar changes in the frequencies with leaching time by an initial increase (from 1 to 7 days), followed by a gradual decrease until 28 days. This suggests that the polymerization degree of the C-(N-)A-S-H gels initially increases and then decreases during 28 days of water immersion, possibly as a result of a loss and redistribution of cations during leaching. However, the decrease in wavenumbers upon prolonged leaching is smaller than the initial increase during the first days (Fig. 7), suggesting that the gels after leaching for 28 days are more cross-linked as compared to the structures before leaching. These findings align well with our recent study on alkali-activated slag pastes subjected to water immersion [9] and are further supported by the NMR results in the following section.

3.3.2. NMR

The low crystallinity of the C-(N-)A-S-H gels poses challenges in the quantitative structural analysis of these phases using conventional powder XRD and FTIR techniques. For such phases with lacking long-range order, solid-state NMR can often provide more details about the local structure. By ^{29}Si, ^{27}Al, and ^{23}Na MAS NMR, it is possible for C-(N-)A-S-H gels to quantitatively analyze the basic dreierketten chains of silicate units, the presence of tetrahedrally, fivefold- and octahedrally coordinated Al species, and Na ions associated with the structures [12,37,45]. This may result in models that consider the nearest coordination environments, as schematically illustrated in Fig. 8 for a C-(N-)A-S-H gel.

3.3.2.1. ^{29}Si MAS NMR. The ^{29}Si MAS NMR spectra of the C-(N-)A-S-H gels before leaching and after water immersion for 28 days are shown in Fig. 9 and are all dominated by three resonances at approx. −79.5 ppm, −82 ppm, and −85 ppm, which can be assigned to the Q^1 $Q^2(1Al_4)$ and Q^2_p sites, respectively, of the basic structure (see Fig. 8). In addition, less

Table 3
Mean chain length (MCL) of aluminosilicate tetrahedra for the C-(N-)A-S-H gels before and after 28 days of leaching as determined from Eq. (1) using the simulated intensities of the ^{29}Si MAS NMR spectra.

	0.8_0.1_0d	0.8_0.1_28d	0.8_0.3_0d	0.8_0.3_28d	1.2_0.3_0d	1.2_0.3_28d
MCL	13.0	19.2	14.8	16.1	7.5	8.1

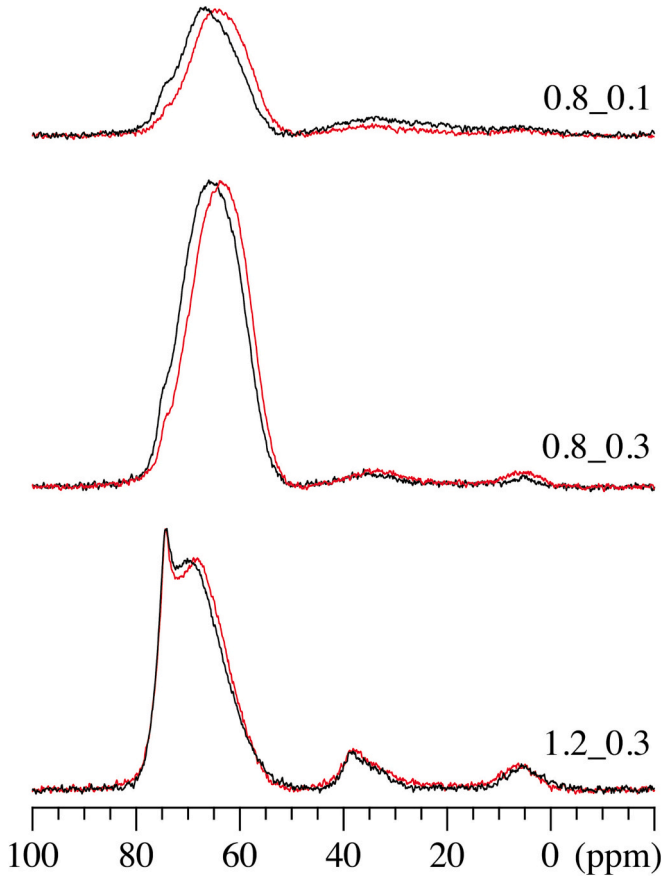

Fig. 12. ^{27}Al NMR spectra (22.3 T, ν_R = 25.0 kHz) of the C-(N-)A-S-H gels before (black) and after 28 days of water immersion (red). (For interpretation of the references to color in this figure legend, the reader is referred to the web version of this article.)

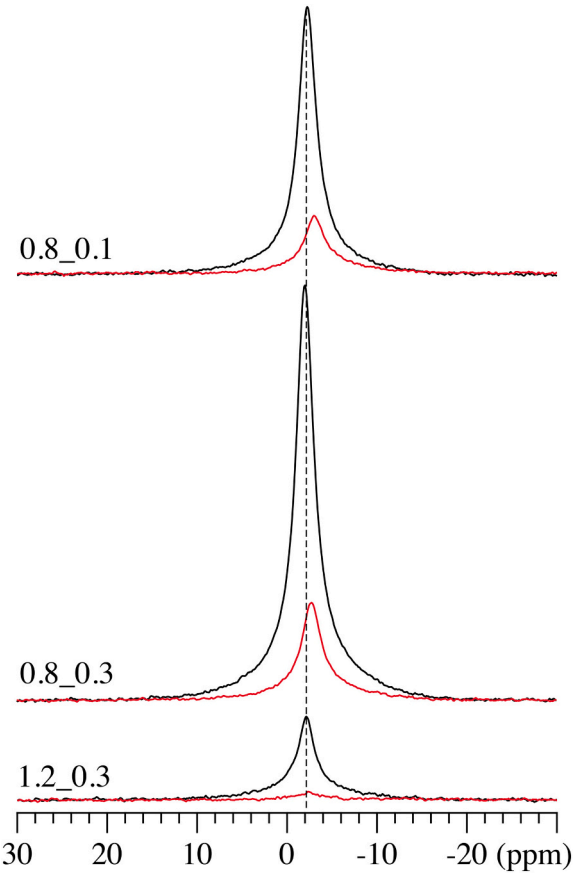

Fig. 13. ^{23}Na NMR spectra (22.3 T, ν_R = 25.0 kHz) of the C-(N-)A-S-H gels before (black) and after 28 days of water immersion (red). (For interpretation of the references to color in this figure legend, the reader is referred to the web version of this article.)

resolved peaks and shoulders are observed at lower frequencies, which may originate from Q^3(1Al) (~−90 ppm) and Q^3 sites (−93 ppm) [12]. The two Q^3 sites have also been reported in ^{29}Si NMR spectra of Al-substituted natural tobermorite [48,49] and synthesized C-(N-)A-S-H phases with a low Ca/Si ratio [13,15,28]. It is noted that a second paired site (Q^2_{pb}; −86.7 ppm), originating from paired sites in the middle of octameric or longer silicate units, has been observed in synthesized C-(A-)S-H phases [37]. However, indications of this site are not seen in the present ^{29}Si NMR spectra (Fig. 9) and thus not included in the analysis. Following the defect tobermorite model for C-(N-)A-S-H gels and C-(A-)S-H phases [37], a resonance from the bridging sites (Q^2_b) sites is also present at roughly −83 ppm, which should exhibit half the intensity of the Q^2_p sites.

The individual ^{29}Si NMR spectra are simulated using resonances from the Q^1, Q^2_p, Q^2_b, $Q^2(1Al_4)$, Q^3 and $Q^3(1Al_4)$ sites, using the same optimized simulation approach as recently described for synthesized C-(A-)S-H phases [37], including the intensity relation $I(Q^2_p)/I(Q^2_b) = 2$. As an example, Fig. 10 shows the optimized simulation and constituent peaks for the 0.8_0.1C-(N-)A-S-H gel after 28 days of water immersion. The simulations of the ^{29}Si MAS NMR spectra provide relative intensities for the six distinct types of SiO_4 sites, which allow estimation of the mean chain length of alumino-silicate tetrahedra (MCL) for the synthesized gels before and after leaching. For MCL we have chosen to include Al_4 and Si in Q^3 sites but only on the side of the chain that they belong to, resulting in the follow expression for MCL:

$$\mathrm{MCL} = \frac{2\left[Q^1 + Q^2 + \frac{3}{2}Q^2(1Al_4) + Q^3 + Q^3(1Al_4)\right]}{Q^1} \quad (1)$$

where $Q^2 = Q^2_p + Q^2_b$. Fig. 11 shows the intensity fractions for the different types of silicate environments, corresponding to the optimized simulations illustrated in Fig. 9, which result in the MCL values listed in Table 3.

The Q^2_p resonance dominates the spectra of the C-(N-)A-S-H gel with a Ca/Si ratio of 0.8, in agreement with the presence of longer silicate chains at a low Ca/Si ratio. Moreover, the higher Al/Si ratio of 0.3 for two of the gels are clearly reflected in higher relative intensity for the $Q^2(1Al_4)$ peak, which before leaching increases for the 0.8_0.1, 0.8_0.3, and 1.2_0.3 gels, respectively, in agreement with the Al/Si ratios of the gels determined by XRF (Fig. 4). Comparison of the ^{29}Si MAS NMR

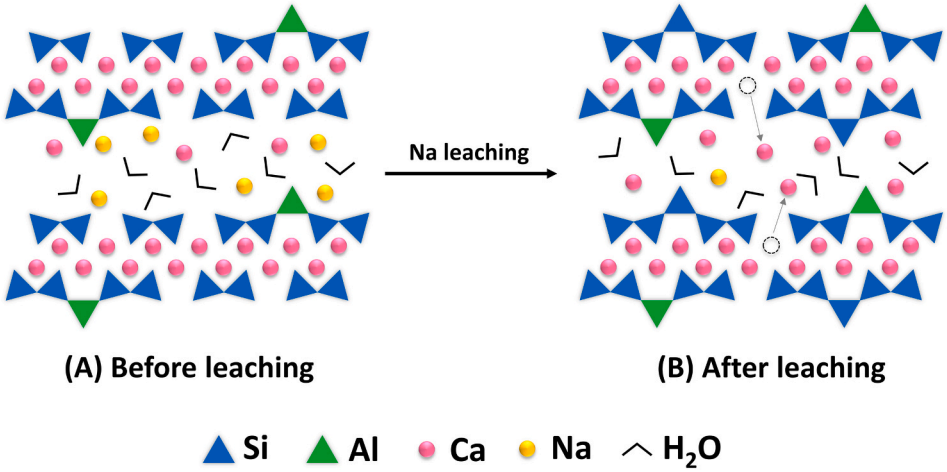

Fig. 14. A schematic model for the impact of Na leaching on the structure of C-(N-)A-S-H gels as a result of water immersion. The oxygen in the Ca-O sheets is not shown and SiO_4 and AlO_4 tetrahedra are shown as triangles.

spectra for the C-(N-)A-S-H gels before and after leaching reveals only minor changes (Fig. 9), indicating that 28 days of water immersion does not significantly alter the main structure of C-(N-)A-S-H gel. The intensities of the Q^2 peaks (Fig. 11) show a small increase for all synthesized gels after water immersion and at the expense of Q^1 sites. These changes are also reflected by an increase in MCLs after leaching (Table 3), which can be ascribed to a decalcification of the C-(N-)A-S-H gels, since an increase in MCL corresponds to a decrease in Ca/Si ratio. The decalcification of C-(N-)A-S-H gels is further supported by the shift of Q^2_p sites from about −85.0 ppm to −85.4 ppm upon leaching, following an earlier ^{29}Si NMR study of C-S-H phases synthesized at different Ca/Si ratios [50]. Interestingly, the increase in MCL upon leaching is notably higher for the C-(N-)A-S-H gel with Al/Si = 0.1 as compared to the gels with Al/Si = 0.3. This suggests that the presence of Al_4 in the chain structure of the C-(N-)A-S-H gels partly hinders decalcification due to leaching. This may reflect that Si substitution by Al in the chains reduces the charge of the gel structure, providing an option for a stronger binding of Ca^{2+} ions.

The presence of Q^3 and Q^3(1Al) sites is consistently observed for all three gels before leaching (Figs. 9 and 11), in agreement with earlier findings from ^{29}Si NMR studies of C-(N-)A-S-H gels in alkali-activated slag pastes [41]. It is notable that the gels with a Ca/Si ratio of 0.8 exhibit higher contents of Q^3 and Q^3(1Al) sites, indicating that a lower Ca/Si ratio promotes the formation of more cross-linked C-(N-)A-S-H gel structures. Furthermore, a small increase in Q^3 and $Q^3(1Al_4)$ intensities is observed after 28 days of exposure, reflecting an increased cross-linking as a result of the observed decalcification of the gels over the leaching period.

3.3.2.2. ^{27}Al MAS NMR. The ^{27}Al MAS NMR spectra for the synthesized C-(N-)A-S-H gels before and after leaching for 28 days are shown in Fig. 12 and reveal distinct centerband resonances for Al in tetrahedral (50–80 ppm), five-fold (30–50 ppm) and octahedral (0–20 ppm) coordination. The observed spectra show no indications of secondary phases, as also suggested by powder XRD (Fig. 3). The spectra are dominated by tetrahedrally coordinated Al sites, as seen by the narrow peak at 74.5 ppm for the 1.2_0.3 gel and by the broad resonance at roughly 65 ppm for all samples. Very low-intensity resonances from Al_5 and Al_6 are observed for the Ca/Si = 0.8 gel, in agreement with our expectations based on recent studies of C-(A-)S-H phases [37,47], whereas they exhibit slightly higher intensity for the Ca/Si = 1.2 gel. This supports our approach to simulate the ^{29}Si NMR spectra (Figs. 9 and 10) which does not consider specific peaks for Si neighbouring Al_5 or Al_6 in the aluminosilicate chains.

The ^{27}Al NMR spectra after 28 days of water exposure exhibit very similar intensities as those obtained before leaching, supporting the earlier findings from XRF (Fig. 4) that Al does not leach out from the C-(N-)A-S-H gel structure. The Al_5 and Al_6 resonances are unaffected by the leaching, whereas small shifts to lower frequency are observed for the broad Al_4 resonances. Previous studies have reported the existence of multiple tetrahedrally coordinated Al sites in C-(A-)S-H phases with Ca/Si ratios ranging from 0.6 to 1.4 and Al/Si ratios up to 0.3 [28,37]. In a recent study [37], three different Al_4 sites were proposed from ^{27}Al MAS and multiple-quantum (MQ) MAS experiments at 14.1 and 22.3 T, all situated in a bridging site but charge-balanced by different ions, i.e., Al_4(a) (centre of gravity δ_{cg} = 75.4 ppm at 22.3 T) – an Al site charge-balanced by a nearby Na^+ ion, Al_4(c) (δ_{cg} = 66.1 ppm) – an Al site charge-balanced by ½ Ca^{2+} ion and H_3O^+, and Al_4(d) (δ_{cg} = 61.3 ppm) – an Al site charged-balanced by interlayer Ca^{2+} ions alone or in conjunction of Na^+ ions. In an earlier study [28], it was proposed that the Al resonance at ~74 ppm represents Al in a bridging site charge-balanced by Al_5 and Al_6 species in the interlayer or on the surface of the C-(A)-S-H gels and that the resonances at ~66 ppm and ~58 ppm originate from AlO_4 Q^2 (i.e., a bridging site) and AlO_4 Q^3 (i.e., a cross-linking site) units, respectively. The narrow resonance at 74.5 ppm, seen in all spectra before leaching and most clearly for the 1.2_0.3 gel, is assigned to the Al_4(a) site whereas the broader Al_4 peak may be a sum of resonances from Al_4 (c), Al_4(d) and cross-linked Q^3 Al. The intensity of the Al_4(a) site is clearly reduced upon leaching for the two gels with Ca/Si = 0.8, whereas the shift of the main resonance to lower frequency (from 65.4 ppm to 64.3 ppm) for the Ca/Si = 0.8 gels suggests a larger interaction with Ca^{2+} ions in the interlayer, following the assignment of the Al_4(c) and Al_4(d) sites. For the C-(N-)A-S-H gel with Ca/Si = 1.2, a shift from 70.1 ppm to 68.6 ppm is also observed for the dominant broad resonance upon leaching. Thus, this shift may reflect an increased role of Ca^{2+} ions in charge balancing the Q^2 and Q^3 AlO_4 sites, when Na ions are removed from the interlayers. It is noted that there are no discernible changes in the relative intensities for the Al_5 and Al_6 resonances before and after leaching, indicating that these Al species are not affected by water leaching when present at relatively low Ca/Si ratios.

3.3.2.3. ^{23}Na MAS NMR. The ^{23}Na NMR spectra of the gels before and after water immersion for 28 days (Fig. 13) all show a featureless resonance for the central transition around −2 ppm with no apparent effects of any second-order quadrupolar broadening. This may reflect that the spectra are acquired at a very high magnetic field (22.3 T) eventually in combination with mobility or dynamic processes for the Na ions present in the C-(N-)A-S-H gels, which average out the second-order quadrupolar interaction. The ^{23}Na NMR spectra are very similar to

those reported in a recent study of synthesized C-(A-)S-H phases [37] and the observed resonance can be assigned to outer-sphere hydrated sodium ions ($[Na(H_2O)_{6-x}]^+$, $x \leq 6$) either adsorbed to the surface of the C-(A-)S-H particles or present in the interlayer of the structure. A small shift to lower frequency is observed after leaching for the two Ca/Si = 0.8 samples, which may reflect a reduction in the number of water molecules on average surrounding the Na^+ ions for example obtained by a stronger binding to silanol groups in the C-(A-)S-H structure. The ^{23}Na NMR spectra of the gels after leaching show a significant decrease in intensities, and thereby unambigously demonstrate that a major part of sodium is removed for the C-(N-)A-S-H structure upon water immersion, in agreement with the bulk results from the XRF measurements (Fig. 4). The ^{23}Na NMR intensities reveal that approximately 70 % of the Na ions (quantified from ^{23}Na NMR spectra) have been leached out from the C-(N-)A-S-H gels with Ca/Si = 0.8 and nearly all sodium for the Ca/Si = 1.2 gel.

3.4. Summary and perspectives

The leaching of ions by water immersion and consequent chemical changes of the gels are accomplished by structural changes of the C-(N-)A-S-H gels, as clearly reflected in the present results from FTIR and solid-state NMR. The polymerization degree of the gels, as reflected by the MCL values (Table 3), increases after water immersion as a result of Na leaching. The leaching process for conventional C-(A-)S-H gels has been investigated in recent studies [18], nevertheless, the underlying mechanism of the impact of Na leaching on structural changes for specific C-(N-)A-S-H gels in AAS systems has not been presented. From the results of the present study, a mechanism is proposed, as schematically presented by the model in Fig. 14.

In alkali-free C-(A-)S-H systems, Ca is the main charge compensator in the interlayer. The introduction of Na can partially take over the charge-compensating role of Ca, resulting in a gel structure where Na is present in the interlayers [12,25,28,33] (Fig. 14A). The Ca ions that are substituted by Na as charge compensators can take part in the formation of the Ca—O sheets, which will lead to a decrease in the fraction of Q^2 sites and thereby shorter average alumino-silicate chains [51]. During water exposure, Na^+ ions are rapidly released from the interlayer, which may result in a structural reorganization where a portion of the Ca ions in the Ca—O sheets migrate to the interlayer and serve the role of charge balancing (Fig. 14B). This mechanism is supported by the ^{27}Al NMR spectra (Fig. 12), where a small shift of the Al(4) resonance to lower frequency is observed upon leaching, which can be assigned to an increasing coordination to Ca^{2+} ions in the second-nearest coordination sphere. The resulting reduction of intralayer Ca^{2+} ions may explain the increase of Q^2 SiO_4 sites [16] and thereby the increased MCL values (Table 3) upon leaching, as also evidenced by the increase of in wavenumbers for the Q^2 sites in the FTIR spectra at the early stages (Fig. 6).

The results from the present work provide novel perspectives for understanding the process of sodium leaching by water immersion. It is widely recognized that the MCLs or polymerization degree of gels is dependent on the Ca content in the intralayer. In previous studies [52,53], it has been reported that a reduction in the fraction of intralayer Ca results in notable volume deformation and reduction in mechanical properties, which commonly occur after the leaching of interlayer Ca. The findings of this study propose that the leaching of interlayer Na can trigger a simultaneous restructuring of intralayer Ca which affects its properties, following earlier reported results [52,53].

4. Conclusions

In this study, we have investigated the leaching behaviour, chemical compositions, and structural transformations of C-(N-)A-S-H gels under water-exposed leaching conditions, using three synthesized C-(N-)A-S-H gels with varying Ca/Si ratios (0.8 and 1.2) and Al/Si ratios (0.1 and 0.3). Our findings reveal that leaching of these synthesized C-(N-)A-S-H gels is a rapid process, which stabilizes within seven days and with minimal formation of secondary phases, except for a minor presence of calcium carbonate in the leached gel with a high Ca/Si ratio of 1.2. Notably, sodium leaches out rapidly and significantly within a few hours, with approximately 70 % of Na leaching out from gels with a Ca/Si ratio of 0.8 after 28 days of water immersion. Conversely, only minimal leaching, if any, is observed for the other elements, with the most notable being calcium (Ca) in the gel with a high Ca/Si ratio.

Interestingly, the gel with the higher Ca/Si ratio of 1.2 experiences only a small degree of decalcification during water immersion, whereas a significant loss of Na is observed for all gels. Both of these processes contribute to an increased polymerization of aluminosilicate tetrahedra within the gel structure. We propose that the mechanism behind the impact of Na leaching on the gel structure is related to the change in charge compensators within the interlayer of the C-(N-)A-S-H gels. As Na leaches out from the interlayer, calcium progressively takes the role of charge compensation, resulting in structural modifications. This proposed mechanism is supported by findings from ^{23}Na, ^{27}Al, and ^{29}Si NMR as well as from FTIR measurements.

CRediT authorship contribution statement

Chen Liu: Writing – review & editing, Writing – original draft, Investigation, Data curation. **Zhenming Li:** Writing – review & editing, Methodology, Conceptualization. **Shuai Nie:** Writing – review & editing, Investigation. **Jørgen Skibsted:** Writing – review & editing, Supervision. **Guang Ye:** Writing – review & editing, Supervision, Funding acquisition, Conceptualization.

Declaration of competing interest

The authors declare that they have no known competing financial interests or personal relationships that could have appeared to influence the work reported in this paper.

Data availability

Data will be made available on request.

Acknowledgement

Chen Liu would like to acknowledge the funding supported by the China Scholarship Council (CSC) under grant No. 201906950102. J. Skibsted thanks the Carlsberg Foundation (No CF14-0138) for an equipment grant and for access to the facilities at the Danish Center for Ultrahigh-Field NMR Spectroscopy funded by the Danish Ministry of Higher Education and Science (Grant no. AU-2010-612-181) and the Novo Nordisk Foundation (Grant no. NNF220C0075797).

Appendix A

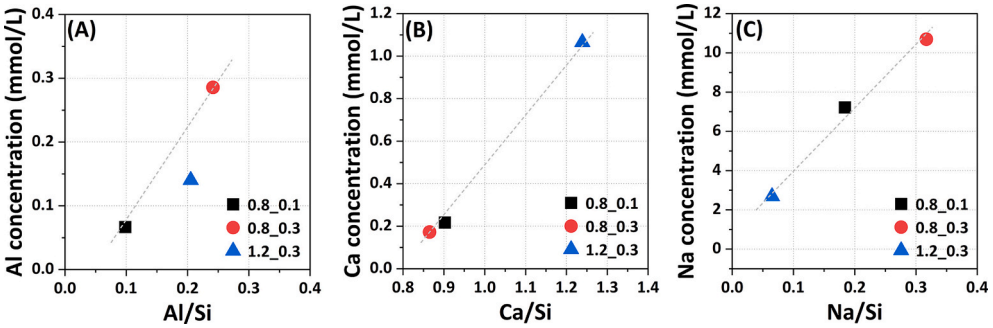

Fig. A1. Relationships between ion concentrations of the leachates for the C-(N-)A-S-H gels after 28 days of water immersion and the cation elemental ratios before leaching of the gels.

References

[1] J.L. Provis, Alkali-activated materials, Cem. Concr. Res. 114 (2018) 40–48, https://doi.org/10.1016/j.cemconres.2017.02.009.

[2] J.L. Provis, S.A. Bernal, Geopolymers and related alkali-activated materials, Annu. Rev. Mat. Res. 44 (2014) 299–327, https://doi.org/10.1146/annurev-matsci-070813-113515.

[3] J.L. Provis, A. Palomo, C. Shi, Advances in understanding alkali-activated materials, Cem. Concr. Res. 78 (2015) 110–125, https://doi.org/10.1016/j.cemconres.2015.04.013.

[4] S.A. Bernal, J.L. Provis, Durability of alkali-activated materials: progress and perspectives, J. Am. Ceram. Soc. 97 (2014) 997–1008, https://doi.org/10.1111/jace.12831.

[5] F. Pacheco-Torgal, Z. Abdollahnejad, A.F. Camões, M. Jamshidi, Y. Ding, Durability of alkali-activated binders: a clear advantage over Portland cement or an unproven issue? Construct. Build Mater. 30 (2012) 400–405, https://doi.org/10.1016/j.conbuildmat.2011.12.017.

[6] Y. Ding, J.G. Dai, C.J. Shi, Mechanical properties of alkali-activated concrete: a state-of-the-art review, Construct. Build Mater. 127 (2016) 68–79, https://doi.org/10.1016/j.conbuildmat.2016.09.121.

[7] X. Yao, T. Yang, Z.Z. Zhang, Y. Wang, X. Liu, W.D. Zhang, Z. Li, Y. Zhang, Y. Li, Y. Ren, K. Sun, X. Peng, S. Wang, L. Zeng, P. Ran, G. Ji, M.A. Longhi, E. D. Rodríguez, B. Walkley, Z.Z. Zhang, A.P. Kirchheim, S.P. Kang, S.J. Kwon, X. Xue, Y.L. Liu, J.G. Dai, C.S. Poon, W.D. Zhang, P. Zhang, Z.Z. Zhang, J.L. Provis, X. Ma, A. Reid, H. Wang, J.L. Provis, A. Reid, X. Yao, T. Yang, Z.Z. Zhang, J.L. Provis, A. Reid, H. Wang, R.R. Lloyd, J.L. Provis, J.S.J. Van Deventer, Compressive strength development and shrinkage of alkali-activated fly ash–slag blends associated with efflorescence, Mater. Struct. 49 (2016) 165–177, https://doi.org/10.1016/j.cemconcomp.2018.06.010.

[8] G. Huang, Y. Ji, L. Zhang, J. Li, Z. Hou, The influence of curing methods on the strength of MSWI bottom ash-based alkali-activated mortars: the role of leaching of OH^- and free alkali, Construct. Build Mater. 186 (2018) 978–985, https://doi.org/10.1016/j.conbuildmat.2018.07.224.

[9] C. Liu, X. Liang, Y. Chen, Z. Li, G. Ye, Degradation of alkali-activated slag subject to water immersion, Cem. Concr. Compos. 142 (2022), https://doi.org/10.1016/j.cemconcomp.2023.105157.

[10] E. Duque-Redondo, P.A. Bonnaud, H. Manzano, A comprehensive review of C-S-H empirical and computational models, their applications, and practical aspects, Cem. Concr. Res. 156 (2022) 106784, https://doi.org/10.1016/j.cemconres.2022.106784.

[11] R.J. Myers, E. L'Hôpital, J.L. Provis, B. Lothenbach, Effect of temperature and aluminium on calcium (alumino)silicate hydrate chemistry under equilibrium conditions, Cem. Concr. Res. 68 (2015) 83–93, https://doi.org/10.1016/j.cemconres.2014.10.015.

[12] R.J. Myers, S.A. Bernal, R. San Nicolas, J.L. Provis, Generalized structural description of calcium-sodium aluminosilicate hydrate gels: the cross-linked substituted tobermorite model, Langmuir 29 (2013) 5294–5306, https://doi.org/10.1021/la4000473.

[13] R.J. Myers, E. L'Hôpital, J.L. Provis, B. Lothenbach, Composition-solubility-structure relationships in calcium (alkali) aluminosilicate hydrate (C-(N,K-)A-S-H), Dalt. Trans. 44 (2015) 13530–13544, https://doi.org/10.1039/c5dt01124h.

[14] I. Garcia-Lodeiro, A. Palomo, A. Fernández-Jiménez, D.E. MacPhee, Compatibility studies between N-A-S-H and C-A-S-H gels. Study in the ternary diagram Na_2O-CaO-Al_2O_3-SiO_2-H_2O, Cem. Concr. Res. 41 (2011) 923–931, https://doi.org/10.1016/j.cemconres.2011.05.006.

[15] Y. Wang, Y. Cao, Z. Zhang, J. Huang, P. Zhang, Y. Ma, H. Wang, Study of acidic degradation of alkali-activated materials using synthetic C-(N)-A-S-H and N-A-S-H gels, Compos. Part B Eng. 230 (2021) 109510, https://doi.org/10.1016/j.compositesb.2021.109510.

[16] N. Garg, V.O. Özçelik, J. Skibsted, C.E. White, Nanoscale ordering and Depolymerization of calcium silicate hydrates in the presence of alkalis, J. Phys. Chem. C 123 (2019) 24873–24883, https://doi.org/10.1021/acs.jpcc.9b06412.

[17] Y. Yan, S.Y. Yang, G.D. Miron, I.E. Collings, E. L'Hôpital, J. Skibsted, F. Winnefeld, K. Scrivener, B. Lothenbach, Effect of alkali hydroxide on calcium silicate hydrate (C-S-H), Cem. Concr. Res. 151 (2022), https://doi.org/10.1016/j.cemconres.2021.106636.

[18] L. Liu, C. Sun, G. Geng, P. Feng, J. Li, R. Dähn, Influence of decalcification on structural and mechanical properties of synthetic calcium silicate hydrate (C-S-H), Cem. Concr. Res. 123 (2019), https://doi.org/10.1016/j.cemconres.2019.105793.

[19] M. Nodehi, T. Ozbakkaloglu, A. Gholampour, T. Mohammed, X. Shi, The effect of curing regimes on physico-mechanical, microstructural and durability properties of alkali-activated materials: a review, Construct. Build Mater. 321 (2022) 126335, https://doi.org/10.1016/j.conbuildmat.2022.126335.

[20] K.C. Reddy, K.V.L. Subramaniam, Investigation on the roles of solution-based alkali and silica in activated low-calcium fly ash and slag blends, Cem. Concr. Compos. 123 (2021) 104175, https://doi.org/10.1016/j.cemconcomp.2021.104175.

[21] M. Ben Haha, B. Lothenbach, G. Le Saout, F. Winnefeld, Influence of slag chemistry on the hydration of alkali-activated blast-furnace slag - part II: effect of Al_2O_3, Cem. Concr. Res. 42 (2012) 74–83, https://doi.org/10.1016/j.cemconres.2011.08.005.

[22] M. Ben Haha, G. Le Saout, F. Winnefeld, B. Lothenbach, Influence of activator type on hydration kinetics, hydrate assemblage and microstructural development of alkali-activated blast furnace slags, Cem. Concr. Res. 41 (2011) 301–310, https://doi.org/10.1016/j.cemconres.2010.11.016.

[23] M. Ben Haha, B. Lothenbach, G. Le Saout, F. Winnefeld, Influence of slag chemistry on the hydration of alkali-activated blast-furnace slag - part I: effect of MgO, Cem. Concr. Res. 41 (2011) 955–963, https://doi.org/10.1016/j.cemconres.2011.05.002.

[24] L. Gomez-Zamorano, M. Balonis, B. Erdemli, N. Neithalath, G. Sant, C–(N)–S–H and N–A–S–H gels: compositions and solubility data at 25°C and 50°C, J. Am. Ceram. Soc. 100 (2017) 2700–2711, https://doi.org/10.1111/jace.14715.

[25] J.J. Chen, J.J. Thomas, H.F.W. Taylor, H.M. Jennings, Solubility and structure of calcium silicate hydrate, Cem. Concr. Res. 34 (2004) 1499–1519, https://doi.org/10.1016/j.cemconres.2004.04.034.

[26] M. Martín-Garrido, M. Teresa Molina-Delgado, S. Martínez-Ramírez, A comparison between experimental and theoretical Ca/Si ratios in C–S–H and C–S(A)–H gels, J. Sol-Gel Sci. Technol. 94 (2020) 11–21, https://doi.org/10.1007/s10971-019-05097-x.

[27] I. García-Lodeiro, A. Fernández-Jiménez, M.T. Blanco, A. Palomo, FTIR study of the sol-gel synthesis of cementitious gels: C-S-H and N-A-S-H, J. Sol-Gel Sci. Technol. 45 (2008) 63–72, https://doi.org/10.1007/s10971-007-1643-6.

[28] G.K. Sun, J.F. Young, R.J. Kirkpatrick, The role of Al in C-S-H: NMR, XRD, and compositional results for precipitated samples, Cem. Concr. Res. 36 (2006) 18–29, https://doi.org/10.1016/j.cemconres.2005.03.002.

[29] W. Hunnicutt, L. Struble, P. Mondal, Effect of synthesis procedure on carbonation of calcium-silicate-hydrate, J. Am. Ceram. Soc. 100 (2017) 3736–3745, https://doi.org/10.1111/jace.14899.

[30] A. Gruskovnjak, B. Lothenbach, L. Holzer, R. Figi, F. Winnefeld, Hydration of alkali-activated slag: comparison with ordinary Portland cement, Adv. Cem. Res. 18 (2006) 119–128.

[31] M. Martín-Garrido, M. Teresa Molina-Delgado, S. Martínez-Ramírez, A comparison between experimental and theoretical Ca/Si ratios in C–S–H and C–S(A)–H gels, J. Sol-Gel Sci. Technol. 94 (2020) 11–21, https://doi.org/10.1007/s10971-019-05097-x.

[32] Y. Zuo, M. Nedeljković, G. Ye, Pore solution composition of alkali-activated slag/fly ash pastes, Cem. Concr. Res. 115 (2019) 230–250, https://doi.org/10.1016/j.cemconres.2018.10.010.

[33] E. L'Hôpital, B. Lothenbach, G. Le Saout, D. Kulik, K. Scrivener, Incorporation of aluminium in calcium-silicate-hydrates, Cem. Concr. Res. 75 (2015) 91–103, https://doi.org/10.1016/j.cemconres.2015.04.007.

[34] J. Skibsted, J. Hjorth, H.J. Jakobsen, Correlation between ^{29}Si NMR chemical shifts and mean SiO bond lengths for calcium silicates, Chem. Phys. Lett. 172 (1990) 279–283, https://doi.org/10.1016/0009-2614(90)85403-Y.
[35] S. Nie, R.M. Thomsen, J. Skibsted, Impact of mg substitution on the structure and pozzolanic reactivity of calcium aluminosilicate ($CaO-Al_2O_3-SiO_2$) glasses, Cem. Concr. Res. 138 (2020) 106231, https://doi.org/10.1016/j.cemconres.2020.106231.
[36] F. Škvára, V. Šmilauer, P. Hlaváček, L. Kopecký, Z. Cílová, A weak alkali bond in (N, K)-A-S-H gels: evidence from leaching and modeling, Ceram. - Silikaty. 56 (2012) 374–382.
[37] S.Y. Yang, Y. Yan, B. Lothenbach, J. Skibsted, Incorporation of sodium and aluminum in cementitious calcium-alumino-silicate-hydrate C-(a)-S-H phases studied by ^{23}Na, ^{27}Al, and ^{29}Si MAS NMR spectroscopy, J. Phys. Chem. C 125 (2021) 27975–27995, https://doi.org/10.1021/acs.jpcc.1c08419.
[38] S. Merlino, E. Bonaccorsi, T. Armbruster, The real structure of tobermorite 11 Å: normal and anomalous forms, OD character and polytypic modifications, Eur. J. Mineral. 13 (2001) 577–590.
[39] E. L'Hôpital, B. Lothenbach, D.A. Kulik, K. Scrivener, Influence of calcium to silica ratio on aluminium uptake in calcium silicate hydrate, Cem. Concr. Res. 85 (2016) 111–121, https://doi.org/10.1016/j.cemconres.2016.01.014.
[40] E. Kapeluszna, Ł. Kotwica, A. Różycka, Ł. Gołek, Incorporation of Al in C-A-S-H gels with various Ca/Si and Al/Si ratio: microstructural and structural characteristics with DTA/TG, XRD, FTIR and TEM analysis, Construct. Build Mater. 155 (2017) 643–653, https://doi.org/10.1016/j.conbuildmat.2017.08.091.
[41] R.J. Myers, S.A. Bernal, J.D. Gehman, J.S.J. Van Deventer, J.L. Provis, The role of al in cross-linking of alkali-activated slag cements, J. Am. Ceram. Soc. 98 (2015) 996–1004, https://doi.org/10.1111/jace.13360.
[42] N.V. Chukanov, IR Spectra of Minerals and Reference Samples Data, Infrared Spectra Miner. Species, Springer, 2014, pp. 21–1701.
[43] A. Vidmer, G. Sclauzero, A. Pasquarello, Infrared spectra of jennite and tobermorite from first-principles, Cem. Concr. Res. 60 (2014) 11–23, https://doi.org/10.1016/j.cemconres.2014.03.004.
[44] M. Król, P. Rożek, D. Chlebda, W. Mozgawa, Influence of alkali metal cations/type of activator on the structure of alkali-activated fly ash – ATR-FTIR studies, Spectrochim. Acta - Part A Mol. Biomol. Spectrosc. 198 (2018) 33–37, https://doi.org/10.1016/j.saa.2018.02.067.
[45] P. Yu, R.J. Kirkpatrick, B. Poe, P.F. McMillan, X. Cong, Structure of calcium silicate hydrate (C-S-H): near-, mid-, and far-infrared spectroscopy, J. Am. Ceram. Soc. 82 (1999) 742–748.
[46] Z. Zhang, H. Wang, J.L. Provis, F. Bullen, A. Reid, Y. Zhu, Quantitative kinetic and structural analysis of geopolymers. Part 1. the activation of metakaolin with sodium hydroxide, Thermochim. Acta 539 (2012) 23–33, https://doi.org/10.1016/j.tca.2012.03.021.
[47] A. Kunhi Mohamed, P. Moutzouri, P. Berruyer, B.J. Walder, J. Siramanont, J. Siramanont, M. Harris, M. Negroni, S.C. Galmarini, S.C. Parker, S.C. Parker, K. L. Scrivener, L. Emsley, P. Bowen, The atomic-level structure of cementitious calcium aluminate silicate hydrate, J. Am. Chem. Soc. 142 (2020) 11060–11071, https://doi.org/10.1021/jacs.0c02988.
[48] M. Sakiyama, Synthesis and Crystal Chemistry of Al - Substituted 11 Å Tobermorite MAESHIMA and Takeshi MITSUDA 419, 2000, pp. 413–419.
[49] T. Maeshima, H. Noma, M. Sakiyama, T. Mitsuda, Natural 1.1 and 1.4 nm tobermorites from Fuka, Okayama, Japan: chemical analysis, cell dimensions, ^{29}Si NMR and thermal behavior, Cem. Concr. Res. 33 (2003) 1515–1523, https://doi.org/10.1016/S0008-8846(03)00099-1.
[50] T.F. Sevelsted, J. Skibsted, Carbonation of C-S-H and C-A-S-H samples studied by ^{13}C, ^{27}Al and ^{29}Si MAS NMR spectroscopy, Cem. Concr. Res. 71 (2015) 56–65, https://doi.org/10.1016/j.cemconres.2015.01.019.
[51] F. Puertas, M. Palacios, H. Manzano, J.S. Dolado, A. Rico, J. Rodríguez, A model for the C-A-S-H gel formed in alkali-activated slag cements, J. Eur. Ceram. Soc. 31 (2011) 2043–2056, https://doi.org/10.1016/j.jeurceramsoc.2011.04.036.
[52] Y. Zhang, L. Guo, J. Shi, Q. Luo, J. Jiang, D. Hou, Full process of calcium silicate hydrate decalcification: molecular structure, dynamics, and mechanical properties, Cem. Concr. Res. 161 (2022) 106964, https://doi.org/10.1016/j.cemconres.2022.106964.
[53] M. Jin, Y. Ma, W. Li, J. Huang, Y. Yan, H. Zeng, C. Lu, J. Liu, Multi-scale investigation on composition-structure of C-(A)-S-H with different Al/Si ratios under attack of decalcification action, Cem. Concr. Res. 172 (2023), https://doi.org/10.1016/j.cemconres.2023.107251.